Optical force on toroidal nanostructures: Toroidal dipole versus renormalized electric dipole

Xu-Lin Zhang,[1,2] S. B. Wang,[1] Zhifang Lin,[3,4] Hong-Bo Sun,[2] and C. T. Chan[1,*]

[1]*Department of Physics and Institute for Advanced Study, The Hong Kong University of Science and Technology, Clear Water Bay, Hong Kong, China*

[2]*State Key Laboratory on Integrated Optoelectronics, College of Electronic Science and Engineering, Jilin University, Changchun, China*

[3]*State Key Laboratory of Surface Physics and Key Laboratory of Micro and Nano Photonics Structure (Ministry of Education), Fudan University, Shanghai 200433, China*

[4]*Collaborative Innovation Center of Advanced Microstructures, Fudan University, Shanghai 200433, China*

(Received 15 May 2015; published 2 October 2015)

We study the optical forces acting on toroidal nanostructures. A great enhancement of optical force is unambiguously identified as originating from the toroidal dipole resonance based on the source representation, where the distribution of the induced charges and currents is characterized by the three families of electric, magnetic, and toroidal multipoles. On the other hand, the resonant optical force can also be completely attributed to an electric dipole resonance in the alternative field representation, where the electromagnetic fields in the source-free region are expressed by two sets of electric and magnetic multipole fields based on symmetry. The confusion is resolved by conceptually introducing the irreducible electric dipole, toroidal dipole, and renormalized electric dipole. We demonstrate that the optical force is a powerful tool to identify toroidal response even when its scattering intensity is dwarfed by the conventional electric and magnetic multipoles.

DOI: 10.1103/PhysRevA.92.043804 PACS number(s): 42.50.Wk, 42.50.Ct, 78.67.Pt, 78.67.Sc

I. INTRODUCTION

The notions of toroidal multipoles have been widely used in different disciplines of physics [1–7]. The simplest model for a toroidal dipole can be visualized as current flowing on the surface of a torus along its meridians. Such complex current distributions are difficult to excite but thanks to recent advances in material fabrication [8–10], toroidal metamaterials were theoretically predicted [11] and experimentally demonstrated at microwave frequencies [12], followed by various studies on their intriguing properties [13–19]. The requirement of introducing the notion of toroidal multipoles is due to the fact that a general type of charge or current distribution, either free or induced, cannot be represented exclusively by the standard electric and magnetic multipoles as defined in textbooks. From the mathematical point of view, the current is a vector with three independent components, while the charge is a scalar. With the continuity equation, one needs three functionals to characterize a general type of source, corresponding to three families of multipoles. This constitutes the source representation, so termed as it focuses on parametrizing the source, with the source being either free or induced charge or current. On the other hand, a divergenceless vector function can be expanded in terms of two sets of multipole fields, termed the electric and magnetic multipole fields, described by vector spherical functions [20], with the expansion coefficients designated as electric and magnetic multipole coefficients (see, e.g., [21]). This forms the field representation since it focuses on the radiated fields. The electromagnetic fields in the source-free region can be defined in the field representation based on electric and magnetic multipoles, without resorting to the third type of toroidal multipole [20–23]. This naturally leads to a question as to whether toroidal excitation is indispensable to characterize the electromagnetic fields. This issue has been largely ignored since the toroidal excitation is typically obscured by much stronger electric or magnetic multipole excitations. But with more and more "toroidal excitations" being reported in the literature, it is highly desirable that we can reconcile the source representation and the field representation.

In this paper, we clarify this issue by studying the optical forces acting on complex nanostructures that support strong toroidal excitations. On one hand, the optical force acting on an object can produce a measurable physical consequence that has been extensively employed to manipulate small particles [24–32]. On the other hand, it can be theoretically calculated either in the source representation, by the interaction between the external fields and the *three* families of multipoles induced on the object or in the field representation, through the coupling between the incident fields and the *two* types of multipole excited on the scatterer. Hence, it serves as a good platform to address the aforementioned confusion. We will show that the expansions of the optical force on a nanostructure based on the source and field representations result in different multipole moments: an irreducible dipole, a toroidal dipole, and a renormalized dipole. While the toroidal dipole is necessary for the description of optical forces in the source representation and may overwhelmingly dominate the optical force when toroidal dipole resonance is excited, its role is entirely attributed to the renormalized electric dipole resonance in the field representation. As a consequence, although the field representation facilitates the solution of a light scattering problem, as has been enjoyed in the T-matrix method [33], the inclusion of the third family of toroidal multipoles may give a more transparent physical picture for understanding the optical force as a consequence of external fields interacting with nanostructures. More importantly, we will show that the optical force can serve as a definitive quantity for the detection of toroidal response in nanostructures even when its scattering intensity is completely overwhelmed by the conventional electric and magnetic multipoles.

*Corresponding author: phchan@ust.hk

II. SOURCE AND FIELD REPRESENTATIONS OF OPTICAL FORCES

We start by considering an object illuminated by a time-harmonic incident wave in vacuum. The time-averaged optical force acting on the object can be written as an integral over a closed spherical surface S_∞ with radius $R_S \to \infty$ [27,30],

$$\langle \mathbf{F}^{\text{exact}} \rangle = -\frac{1}{c}\oint_{S_\infty} [\langle \mathbf{S} \rangle - \langle \mathbf{S}_i \rangle] d\sigma = -\frac{1}{c}\oint_{S_\infty} [\langle \mathbf{S}_{\text{mix}} \rangle + \langle \mathbf{S}_s \rangle] d\sigma, \tag{1}$$

where c is the speed of light in vacuum, $\langle \mathbf{S} \rangle = \frac{1}{2}\text{Re}[\mathbf{E} \times \mathbf{H}^*]$, $\langle \mathbf{S}_i \rangle = \frac{1}{2}\text{Re}[\mathbf{E}_i \times \mathbf{H}_i^*]$, $\langle \mathbf{S}_{\text{mix}} \rangle = \frac{1}{2}\text{Re}[\mathbf{E}_i \times \mathbf{H}_s^* + \mathbf{E}_s \times \mathbf{H}_i^*]$, and $\langle \mathbf{S}_s \rangle = \frac{1}{2}\text{Re}[\mathbf{E}_s \times \mathbf{H}_s^*]$ are the time-averaged Poynting-vector-like terms, with $\mathbf{E}_i$ ($\mathbf{H}_i$) and $\mathbf{E}_s$ ($\mathbf{H}_s$) denoting, respectively, the incident and scattered electric (magnetic) fields. The force in Eq. (1) is formally "exact" provided that the scattered fields are known.

In the source representation, the scattered field from the object is written in terms of the vector potential depending on the induced current density $\mathbf{J}(\mathbf{r}')e^{i\omega R/c}$ on the object, $\mathbf{A}(\mathbf{r}) = \frac{\mu_0}{(4\pi)}\int_V [\mathbf{J}(\mathbf{r}')e^{i\omega R/c}/R] dv'$, where ω is the angular frequency, μ_0 is the free space permeability, $R = |\mathbf{r} - \mathbf{r}'|$, and the time dependence $e^{-i\omega t}$ has been assumed and suppressed. The vector potential can be further Taylor expanded into primitive multipole terms, with the first few moments expressed as [22]

$$\begin{aligned} p_i &= -\frac{1}{i\omega}\int_V J_i dv', \quad m_i = \frac{1}{2}\int_V (\mathbf{r}' \times \mathbf{J})_i dv', \\ q_{ij}^{(e)} &= -\frac{1}{i\omega}\int_V (r'_i J_j + J_i r'_j) dv', \quad q_{ij}^{(m)} = \frac{2}{3}\int_V (\mathbf{r}' \times \mathbf{J})_i r'_j dv', \end{aligned} \tag{2}$$

which are the Cartesian components of the primitive electric dipole moment ($\mathbf{p}$), the primitive magnetic dipole moment ($\mathbf{m}$), the primitive electric quadrupole moment ($\mathbf{q}^{(e)}$), and the primitive magnetic quadrupole moment ($\mathbf{q}^{(m)}$), respectively. These primitive multipoles are actually not widely used because they are nontraceless and asymmetric. One usually extracts the irreducible parts from the primitive multipoles, and attributes the remaining terms to the toroidal multipoles, leading to the irreducible electric and magnetic multipoles, with a few lowest-order moments given by p_i and m_i in Eq. (2), and

$$\begin{aligned} Q_{ij}^{(e)} &= -\frac{1}{i\omega}\int_V \left(r'_i J_j + J_i r'_j - \frac{2}{3}(\mathbf{r}' \cdot \mathbf{J})\delta_{ij} \right) dv', \\ Q_{ij}^{(m)} &= \frac{1}{3}\int_V [(\mathbf{r}' \times \mathbf{J})_i r'_j + (\mathbf{r}' \times \mathbf{J})_j r'_i] dv', \\ t_i &= \frac{1}{10}\int_V [(\mathbf{r}' \cdot \mathbf{J})\mathbf{r}' - 2(\mathbf{r}' \cdot \mathbf{r}')\mathbf{J}]_i dv', \end{aligned} \tag{3}$$

where $Q^{(e)}$, $Q^{(m)}$, and $\mathbf{t}$ are the Cartesian components of the irreducible electric quadrupole moment, the irreducible magnetic quadrupole moment, and the toroidal dipole moment, respectively. We note that the irreducible electric and magnetic dipoles and the primitive ones are the same but they are different for higher-order moments such as quadrupole moments (e.g., $Q_{ij}^{(e)}$ versus $q_{ij}^{(e)}$).

With the multipole moments determined by the induced current density, the time-averaged optical force in Eq. (1) for a nanostructure can be written as a sum [27,30] of the incident forces $\mathbf{F}^{\mathbf{p}}$, $\mathbf{F}^{\mathbf{m}}$, and $\mathbf{F}^{\mathbf{t}}$, due to the direct interaction between the incident fields and the irreducible electric and magnetic dipoles $\mathbf{p}$ and $\mathbf{m}$ and the toroidal dipole $\mathbf{t}$, and the recoil force $\mathbf{F}^{\text{int}}$ [30] resulting from dipole interference,

$$\begin{aligned} \mathbf{F}^{\mathbf{p}} &= \frac{1}{2}\text{Re}[(\nabla \mathbf{E}_i^*) \cdot \mathbf{p}], \\ \mathbf{F}^{\mathbf{m}} &= \frac{1}{2}\text{Re}[(\nabla \mathbf{B}_i^*) \cdot \mathbf{m}], \\ \mathbf{F}^{\mathbf{t}} &= -\frac{k}{2c}\text{Im}[(\nabla \mathbf{E}_i^*) \cdot \mathbf{t}], \\ \mathbf{F}^{\text{int}} &= -\frac{k^4}{12\pi\varepsilon_0 c}\text{Re}[\mathbf{p} \times \mathbf{m}^*] + \frac{k^5}{12\pi\varepsilon_0 c^2}\text{Im}[\mathbf{m} \times \mathbf{t}^*], \end{aligned} \tag{4}$$

where k and ε_0 are, respectively, the wave vector and the free space permittivity. Here, we are only concerned only with the optical force in the k direction and we focus only on the dipole terms in Eq. (4) because they dominate the force acting on a subwavelength nanostructure.

In the field representation, one starts by expanding the scattered field directly in terms of the outgoing and divergenceless vector spherical functions $\mathbf{N}_{mn}^{(3)}(k,\mathbf{r})$ and $\mathbf{M}_{mn}^{(3)}(k,\mathbf{r})$ as [20,23,33,34] $\mathbf{E}_s = \sum_{n,m} iE_{mn}[a_{mn}\mathbf{N}_{mn}^{(3)}(k,\mathbf{r}) + b_{mn}\mathbf{M}_{mn}^{(3)}(k,\mathbf{r})]$ and $\mathbf{H}_s = \frac{k}{\omega\mu_0}\sum_{n,m} E_{mn}[b_{mn}\mathbf{N}_{mn}^{(3)}(k,\mathbf{r}) + a_{mn}\mathbf{M}_{mn}^{(3)}(k,\mathbf{r})]$. Here a_{mn} and b_{mn} are the scattering coefficients (also known as the electric and magnetic multipole coefficients [21], apart from the different normalization factors) which can be determined by doing a field projection [21,23], and $E_{mn} = |E_0|i^n\sqrt{(2n+1)(n-m)!}/\sqrt{n(n+1)(n+m)!}$ with $|E_0|$ characterizing the intensity of the incident electric field. In the case $n = 1$, the vector spherical functions $\mathbf{N}_{mn}^{(3)}(k,\mathbf{r})$ and $\mathbf{M}_{mn}^{(3)}(k,\mathbf{r})$ differ, respectively, from the standard radiated fields of electric and magnetic dipoles, by a normalization constant. The multipole coefficients a_{mn} and b_{mn} are therefore directly related to the electric and magnetic dipole moments, respectively. This is actually how one derives the dynamic dipole polarizability based on the Mie scattering coefficients [27,30]. The dipoles so defined are distinguished from the irreducible dipoles defined in Eq. (2), as can be readily perceived from the exclusion of the toroidal dipole in the field representation. They are therefore termed "renormalized dipoles."

Inserting the scattered fields into Eq. (1), we can similarly decompose the optical force into incident forces $\mathbf{F}^{\tilde{\mathbf{p}}}$ and $\mathbf{F}^{\tilde{\mathbf{m}}}$, arising from the direct interaction between the incident field and the renormalized dipoles, and the recoil force $\mathbf{F}^{\widetilde{\text{int}}}$, due to the interference of the renormalized dipoles, with its $k(z)$ component written as (see Appendix B)

$$\begin{aligned} F_z^{\tilde{\mathbf{p}}} &= \frac{2\pi\varepsilon_0}{k^2}|E_0|^2 \sum_{n=1,m} \text{Re}[g_{mn}a_{m,n}p_{m,n+1}^* + l_{mn}q_{m,n}a_{m,n}^*], \\ F_z^{\tilde{\mathbf{m}}} &= \frac{2\pi\varepsilon_0}{k^2}|E_0|^2 \sum_{n=1,m} \text{Re}[g_{mn}b_{m,n}q_{m,n+1}^* + l_{mn}p_{m,n}b_{m,n}^*], \\ F_z^{\widetilde{\text{int}}} &= -\frac{4\pi\varepsilon_0}{k^2}|E_0|^2 \sum_{n=1,m} \text{Re}(l_{mn}a_{m,n}b_{m,n}^*), \end{aligned} \tag{5}$$

where $p_{m,n}$ and $q_{m,n}$ are the expansion coefficients for the incident wave in terms of vector spherical functions $g_{mn} = \sqrt{n(n+2)(n-m+1)(n+m+1)}/\sqrt{(n+1)^2(2n+1)(2n+3)}$ and $l_{mn} = m/[n(n+1)]$. Here we use overbars to denote the renormalized dipoles (i.e., $\bar{\mathbf{p}}$,$\bar{\mathbf{m}}$), in comparison with the irreducible dipoles and the toroidal dipole (i.e., $\mathbf{p}$,$\mathbf{m}$,$\mathbf{t}$).

We therefore see that the optical force acting on subwavelength nanostructures can be written as a summation of forces acting on the toroidal dipole as well as the irreducible electric and magnetic dipoles, or interpreted as a summation of forces exerted exclusively on the renormalized electric and magnetic dipoles. We will identify the relationship between the irreducible and renormalized dipoles by performing a numerical study on toroidal nanostructures.

III. OPTICAL FORCE ON TOROIDAL STRUCTURES

We first consider a gold helix shown in Fig. 1(a) which will be used as a basic building block to construct toroidal objects later. In the optical regime, the permittivity of gold can be described by the Drude model with plasma frequency $\omega_p = 2\pi \times 2.175 \times 10^{15}$ Hz and damping frequency $\omega_c = 2\pi \times 6.5 \times 10^{12}$ Hz [35]. Under the incidence of a linearly x-polarized plane wave propagating in the z direction, this structure supports a magnetic dipole resonance. We

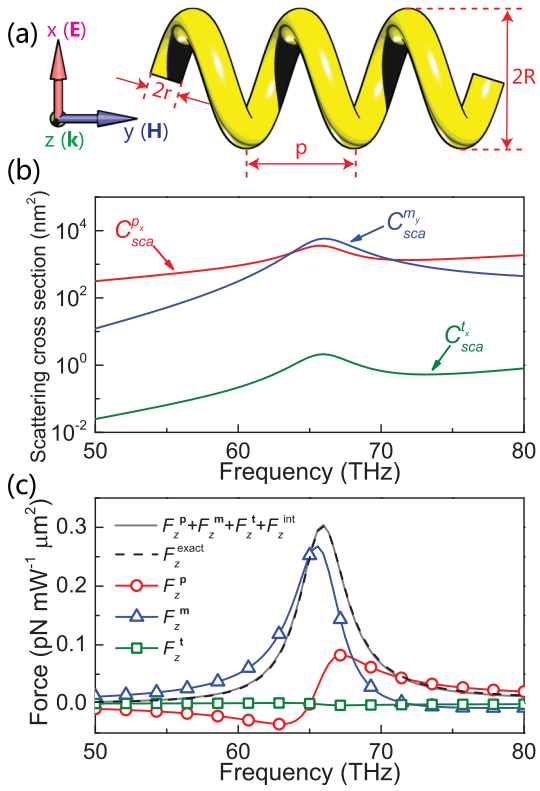

FIG. 1. (Color online) (a) Schematic diagram of a gold helix that supports a magnetic dipole resonance in the optical regime. Structural parameters are inner radius $r = 30$ nm, outer radius $R = 100$ nm, and pitch $p = 200$ nm. (b) Calculated scattering cross sections and (c) z component of optical forces acting on the irreducible dipoles as well as the toroidal dipole in the source representation [Eq. (4)] for the gold helix.

calculate the irreducible dipole moments and the toroidal dipole moment [Eqs. (2) and (3)] using the current density obtained with a finite-element method package COMSOL [36]. Figure 1(b) shows the calculated scattering cross sections (see Appendix A) for some components of the irreducible dipoles and the toroidal dipole in the optical regime. The y component of the irreducible magnetic dipole moment (m_y) exhibits a stronger peak of the scattering cross section at ~66 THz, which coincides with the profile of the z component of the optical forces acting on the irreducible electric and magnetic dipoles and the toroidal dipole, as shown in Fig. 1(c). The resonant force at ~66 THz is mainly contributed by the induced irreducible magnetic dipole moment. The total force acting on all these dipoles ($F_z^{\mathbf{p}} + F_z^{\mathbf{m}} + F_z^{\mathbf{t}} + F_z^{\text{int}}$) could well reproduce the exact result (F_z^{exact}) that is calculated by Eq. (1) using numerically obtained scattered fields [36]. In particular, the effect from the toroidal dipole is completely masked by the irreducible electric and magnetic dipoles, as can be seen from Fig. 1(b), obscuring any distinction between the irreducible and the renormalized dipoles, as in most conventional structures. In other words, the results based on the field representation are found to be graphically indiscernible from those in Figs. 1(b) and 1(c) (that is, $C^{\bar{p}_x}_{\text{sca}} \approx C^{p_x}_{\text{sca}}, C^{\bar{m}_y}_{\text{sca}} \approx C^{m_y}_{\text{sca}}, F_z^{\bar{\mathbf{p}}} \approx F_z^{\mathbf{p}}, F_z^{\bar{\mathbf{m}}} \approx F_z^{\mathbf{m}}$) and are therefore not shown here.

As a toroidal dipole can be represented by a series of magnetic dipoles arranged head to tail along a loop, we can easily obtain a toroidal structure by arranging four helixes into a loop as shown in Fig. 2(a). The corresponding toroidal dipole resonance can be excited by an incident linearly x-polarized plane wave propagating in the z direction. We first use the source representation, in which case the response of the structure can be described by the irreducible dipoles and the toroidal dipole. The calculated scattering cross sections for these induced dipole moments are shown in Fig. 2(c). Only the components that contribute to the incident force are shown here, that is, p_x, m_y, and t_x. Two noticeable resonant peaks (at ~64 THz and ~71 THz) are identified, which originate from the m_y and t_x resonances, respectively. The current density distribution for the resonance at ~71 THz is illustrated in Fig. 2(b), where the threading of the magnetic field lines (black lines) around the structure confirms the excitation of a toroidal dipole resonance [12]. We then show the z component of the optical forces in Fig. 2(d), with two peaks at frequencies coinciding with those of the scattering cross sections in Fig. 2(c). The resonant force at ~64 THz can be attributed to the irreducible magnetic dipole moment m_y while the one at ~71 THz can mainly be associated with the toroidal dipole moment t_x. This provides good evidence that the toroidal dipole is an indispensable part in the multipole expansion based on the source representation. The toroidal-dipole-induced forces in other similar structures (e.g., formed by changing the handedness of the helixes) are also studied and can be found in Fig. 3. We note that, regardless of the handedness of the helix, the toroidal dipole resonance can always be identified and can be associated with a predominant contribution to the optical forces if we take the viewpoint that the optical force acting on an object is a consequence of the incident field interacting with charge or current distributions induced on the object.

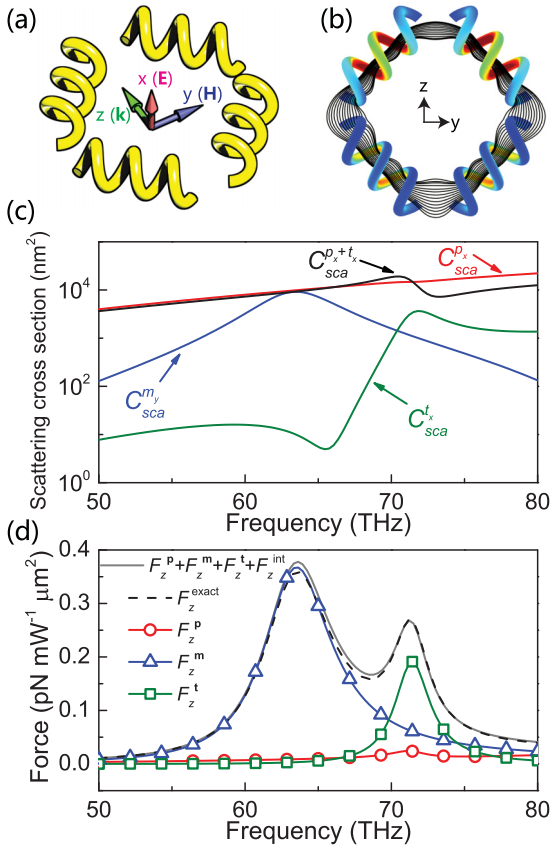

FIG. 2. (Color online) (a) Schematic diagram of the designed nanostructure that supports a toroidal dipole resonance. (b) The intensity distribution of the current density associated with magnetic field lines (black lines) for the toroidal dipole resonance at ∼71 THz. (c) Calculated scattering cross sections and (d) z component of optical forces based on the source representation. The toroidal response manifests itself through a resonant peak in the total optical force at ∼71 THz.

We now use the field representation. We first calculate the partial scattering cross sections (see Appendix A) from each renormalized dipole and the results are shown in Fig. 4(a). We note that at ∼64 THz and ∼71 THz, resonances of a renormalized magnetic dipole $\bar{m}_y$ and a renormalized electric dipole $\bar{p}_x$ are identified respectively. We then calculate the optical forces using Eq. (5) with the coefficients a_{mn}, b_{mn}, p_{mn}, and q_{mn} evaluated by field projections (see Appendix B). Figure 4(b) shows that the strong enhancement of force at the resonance of ∼71 THz is contributed by $F_z^{\bar{\mathbf{p}}}$, a force that comes from the interaction between the incident field and the renormalized electric dipole moment, while the same resonance force in the source representation has been interpreted in Fig. 2(d) as a summation of the contributions from the irreducible electric dipole and the toroidal dipole, with a major part from the toroidal dipole. In addition, the resonance at ∼64 THz in Fig. 4(b) can be attributed to the renormalized magnetic dipole, in agreement with the interpretation in Fig. 2(d). By comparing the force contributions between the two representations [see Figs. 2(d) and 4(b)], we can infer relationships between the optical forces on these dipoles as $\mathbf{F^p} + \mathbf{F^t} \approx \mathbf{F^{\bar{p}}}$ and $\mathbf{F^m} \approx \mathbf{F^{\bar{m}}}$. Actually, the electric far-field

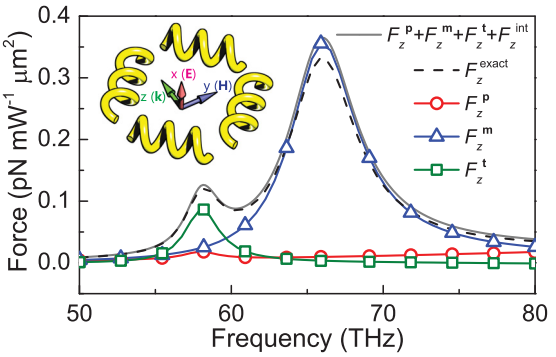

FIG. 3. (Color online) Calculated z component of the optical forces in the optical regime acting on the irreducible dipoles and the toroidal dipole based on the source representation. The inset of the figure illustrates the studied toroidal structure with a different selection of the helical handedness compared to the one in Fig. 2(a).

radiation from the irreducible electric dipole and the toroidal dipole can be written as $\mathbf{n} \times (\mathbf{p} \times \mathbf{n})$ and $(ik/c)\mathbf{n} \times (\mathbf{t} \times \mathbf{n})$, respectively, multiplied by the same factor $k^2 e^{ikr}/(4\pi\varepsilon_0 r)$, with $\mathbf{n}$ denoting the radial direction [30]. The fact that the irreducible electric dipole and the toroidal dipole have a similar form in the expression of the radiation field indicates that the dipoles in the two representations can be related by, at least for the long-wavelength condition, $\mathbf{p} + (ik/c)\mathbf{t} = \bar{\mathbf{p}}$ and $\mathbf{m} = \bar{\mathbf{m}}$. In the far field, one cannot tell whether the radiation field comes from an irreducible electric dipole or a toroidal dipole, but only find a renormalized electric dipole instead. However, it may be physically more transparent to distinguish the irreducible electric moments and toroidal moments based on the source representation, since the latter does show some distinct features [19]. We also note that the similarity of the far-field radiation

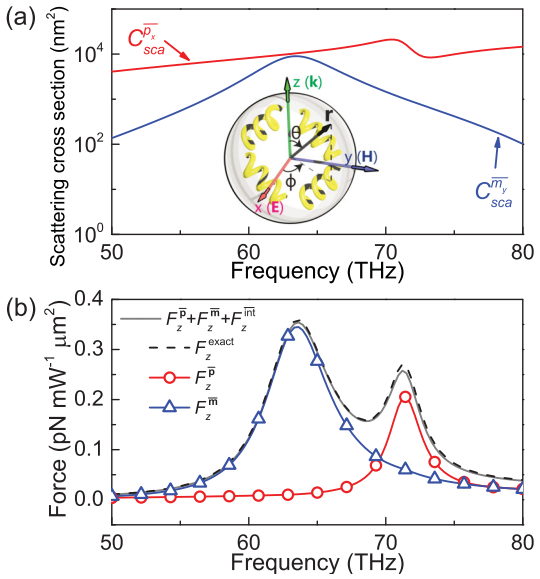

FIG. 4. (Color online) (a) Calculated scattering cross sections and (b) z component of optical forces acting on the renormalized dipoles for the toroidal nanostructure, according to the field representation.

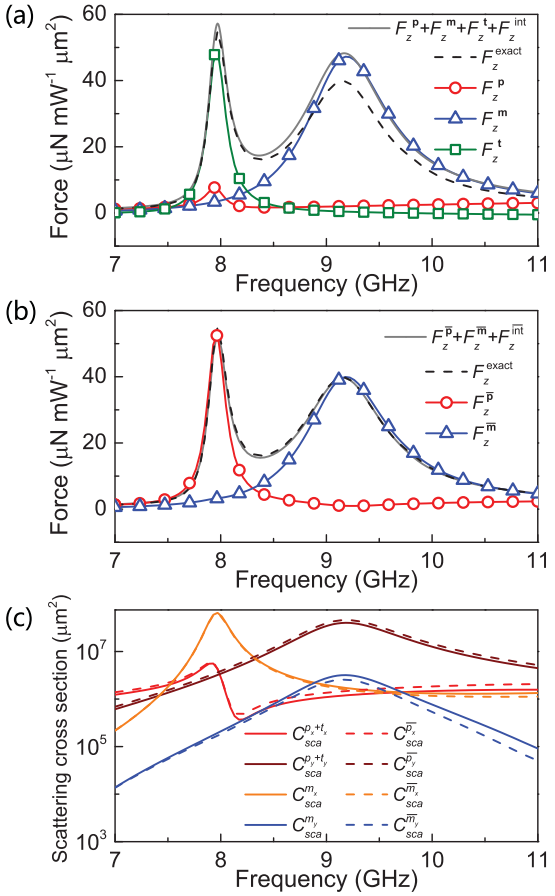

FIG. 5. (Color online) Calculated z component of the optical forces in the microwave regime acting on the toroidal structure (see the inset of Fig. 3) based on (a) source representation and (b) field representation. The parameters are inner radius $r = 0.3$ mm, outer radius $R = 1$ mm, and pitch $p = 2$ mm. (c) Calculated scattering cross sections for the irreducible dipoles, the toroidal dipole, and the renormalized dipoles.

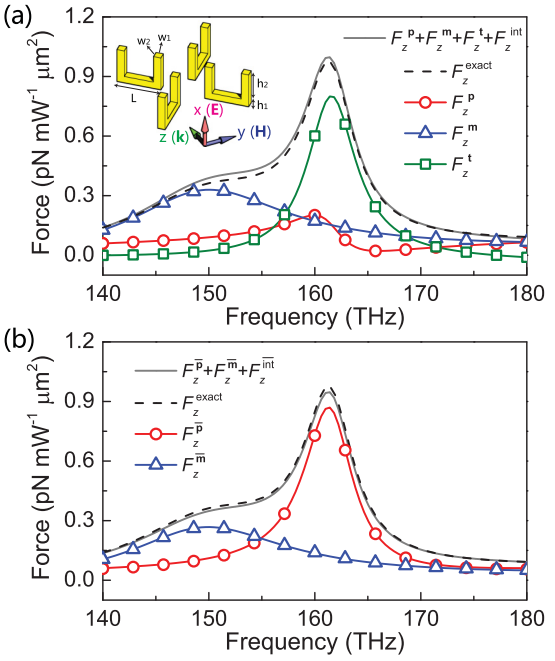

FIG. 6. (Color online) Calculated z component of the optical forces acting on the U-shaped SRRs based toroidal structure based on (a) source representation and (b) field representation. The parameters of each SRR are $L = 300$ nm, $h_1 = w_1 = w_2 = 50$ nm, $h_2 = 200$ nm, and the distance between the structure center and the center of each SRR is 300 nm. The structure is shown in the inset of the top panel. The arrows show the direction of the k vector of the incident plane wave and its polarization. The resonant optical force at slightly above 160 THz can be attributed mainly to a toroidal dipole moment (green line, upper panel) or to the renormalized electric dipole moment (red line, lower panel) depending on how we choose to do the multipole expansion.

pattern of the irreducible electric dipole and the toroidal dipole was very recently exploited to produce "anapoles" [37].

Our theory can also be applied to the microwave regime. We consider the structure shown in the inset of Fig. 3, and change the structure parameters to inner radius $r = 0.3$ mm, outer radius $R = 1$ mm, and pitch $p = 2$ mm. The resonant frequency of the toroidal dipole will then shift to the microwave regime, where the conductivity of gold is $\sigma_{\mathrm{Au}} = 4.098 \times 10^7$ S/m. Figure 5(a) shows the calculated optical forces acting on the irreducible dipoles and the toroidal dipole. We find a strong resonant force at ~8 GHz which can be attributed to the toroidal dipole moment. This resonant force can also be completely accounted for by the renormalized electric dipole, as noted in Fig. 5(b), which shows the optical forces acting on the renormalized dipoles. In Fig. 5(a), there is a slight discrepancy between the force summation ($F_z^{\mathbf{p}} + F_z^{\mathbf{m}} + F_z^{\mathbf{t}} + F_z^{\mathrm{int}}$) and the exact force ($F_z^{\mathrm{exact}}$) in the higher-frequency range, which may be due to the relative large scatterer compared to the resonant wavelength in the microwave regime. Figure 5(c) shows the scattering cross sections for the irreducible dipoles, the toroidal dipole, and the renormalized dipoles, which can support the relations $\mathbf{p} + (ik/c)\mathbf{t} = \bar{\mathbf{p}}$, $\mathbf{m} = \bar{\mathbf{m}}$, for the long-wavelength condition very well, with some discrepancies in the higher-frequency range that can also be attributed to the relatively large scatterer. We also note that the induced dipole moments p_y, t_y, and m_x are even stronger than those (p_x,t_x, and m_y) along the direction of the corresponding incident fields. However, since the oscillating directions of these stronger dipoles are orthogonal with the corresponding incident fields, their contributions to the incident force [see Eq. (4)] are zero.

Our conclusion should be applicable to other systems that support toroidal dipole resonances. We consider a toroidal structure consisting of four U-shaped split ring resonator (SRR) made of gold, as shown in the inset of Fig. 6(a), which has been studied in the literature [13]. Based on the methods introduced above, we calculate the optical forces acting on the SRR-based toroidal structure. The results based on the source representation are given in Fig. 6(a), and those based on the field representation are shown in Fig. 6(b). We find that our conclusion can be supported again by these results. If we view the optical force as a consequence of the interaction between the incident field and induced charge or current distributions [Fig. 6(a)], the force at the resonance at ~160 THz can be attributed to the irreducible electric dipole moment and the

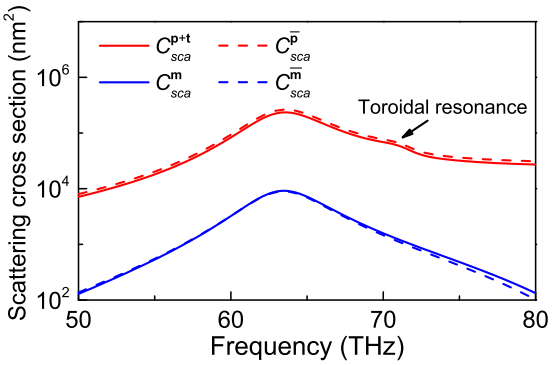

FIG. 7. (Color online) Calculated scattering cross sections for the structure in Fig. 2(a) due to all dipolar components based on source (solid lines) and field (dashed lines) representations.

toroidal dipole moment. From the viewpoint of the field representation [Fig. 6(b)], this resonant force can be attributed to the renormalized electric dipole moment.

IV. DISCUSSION

Conventional transmission or reflection experiments can identify toroidal resonances in purposely designed structures in which the toroidal resonance manifests itself through a significant contribution to the total scattering intensity [12]. In general, toroidal resonances are, however, weak and their contributions to the scattering power are usually obscured by the much stronger irreducible dipoles. In this case, the optical force can serve to detect the toroidal response. To show this point, we plot in Fig. 7 the sum of the scattering cross sections due to all dipolar components (i.e., x,y,z) of the structure shown in Fig. 2(a). The results based on the source representation agree well with those based on the field representation. While the effect of the toroidal dipole on the total scattering cross section is hardly noticeable (the small peak of $C_{\rm sca}^{\rm p+t}$ or $C_{\rm sca}^{\bar{\rm p}}$ at $\sim$71 THz), it gives the dominant contribution to the optical force at $\sim$71 THz [see Fig. 2(d)]. The strong $C_{\rm sca}^{\rm p+t}$ (or $C_{\rm sca}^{\bar{\rm p}}$) here is due to the z component of the corresponding electric dipole, which yields a negligible optical force. The reason that the optical force can reveal the effect of the toroidal dipole is due to the underlying symmetry information incorporated in the force formula. The scattering cross section gives information only about the total number of photons scattered, while the optical force has the extra dependence on the distribution of the scattered photons. Therefore in cases where the scattering cross section of the toroidal dipole is buried in the background and hardly detectable, the toroidal response may still manifest itself through the optical force due to its selectivity in symmetry.

V. SUMMARY

To summarize, we have studied the optical forces acting on toroidal nanostructures based on both the source representation and the field representation. Some confusions in the understanding of various multipoles have been clarified by introducing and distinguishing the primitive multipoles, irreducible multipoles, and renormalized multipoles. A resonant optical force on the toroidal nanostructure can be understood using the source representation as a result of the incident wave interacting with the induced toroidal dipole, or, using the field representation, it is simply interpreted as due to the interaction between the incident field and the renormalized electric dipole. As a consequence, although the field representation expedites the solution of optical scattering problems in many cases, the source representation appears more advantageous for understanding the physics of the optical force. We also show that the optical force enables the observation of the toroidal response of a nanostructure even when its effect on scattering power is overwhelmed by the conventional multipoles. It is also expected to find applications in sorting and selecting nanoparticles with a toroidal response.

ACKNOWLEDGMENTS

We thank Professor Z. Q. Zhang and Professor J. Ng for their valuable comments and suggestions. This work is supported by Hong Kong RGC through Grants No. AOE/P-02/12 and No. CUHK1/CRF/12G-1. Z.L. is supported by NNSFC through Grant No. 11174059 and Ministry of Education of China through Grant No. B06011.

APPENDIX A: CALCULATION OF THE SCATTERING CROSS SECTION

1. For irreducible dipoles and toroidal dipole

Based on the source representation, the radiated powers I from the irreducible dipoles and the toroidal dipole can be written as [12,13]

$$I=\frac{1}{4\pi\varepsilon_0}\left(\frac{2\omega^4}{3c^3}|\mathbf{p}|^2+\frac{2\omega^4}{3c^5}|\mathbf{m}|^2+\frac{4\omega^5}{3c^5}\mathrm{Im}(\mathbf{p}\cdot\mathbf{t}^*)+\frac{2\omega^6}{3c^7}|\mathbf{t}|^2\right), \tag{A1}$$

where ω is the angular frequency. The scattering cross section can be determined by $C_{\rm sca}=2Z_0I/|E_0|^2$, with contributions from the irreducible dipoles and the toroidal dipole as

$$C_{\rm sca}^{\mathbf{p}}=\frac{Z_0\omega^4}{3\pi\varepsilon_0c^3|E_0|^2}|\mathbf{p}|^2,\quad C_{\rm sca}^{\mathbf{m}}=\frac{Z_0\omega^4}{3\pi\varepsilon_0c^5|E_0|^2}|\mathbf{m}|^2,$$
$$C_{\rm sca}^{\mathbf{t}}=\frac{Z_0\omega^6}{3\pi\varepsilon_0c^7|E_0|^2}|\mathbf{t}|^2,\quad C_{\rm sca}^{\mathbf{p+t}}=\frac{Z_0\omega^4}{3\pi\varepsilon_0c^3|E_0|^2}\left|\mathbf{p}+\frac{ik}{c}\mathbf{t}\right|^2, \tag{A2}$$

where Z_0 is the impedance of free space and $|E_0|$ is the magnitude of the incident electric field. The term $C_{\rm sca}^{\mathbf{p+t}}$ denotes the sum of the scattering cross sections contributed by the irreducible electric dipole only ($C_{\rm sca}^{\mathbf{p}}$), the toroidal dipole only ($C_{\rm sca}^{\mathbf{t}}$), and the interference between the two dipoles. Equation (A2) has been used for the calculation of the results in Figs. 1(b), 2(c), 5(c), and 7.

2. For renormalized dipoles

To determine the scattering cross section for the renormalized dipoles, we consider the vector spherical harmonics defined by Bohren and Huffman [23], where even and odd modes were distinguished. The corresponding scattering

coefficients can be worked out using the relations

$$\begin{aligned} A_{emn} &= iE_{mn}[a_{m,n} + (-1)^m a_{-m,n}], \\ A_{omn} &= -E_{mn}[a_{m,n} - (-1)^m a_{-m,n}], \\ B_{emn} &= iE_{mn}[b_{m,n} + (-1)^m b_{-m,n}], \\ B_{omn} &= -E_{mn}[b_{m,n} - (-1)^m b_{-m,n}], \end{aligned} \tag{A3}$$

where the subscripts "e" and "o" denote even and odd, respectively, and

$$E_{mn} = |E_0| i^n \left[\frac{(2n+1)(n-m)!}{n(n+1)(n+m)!}\right]^{1/2}.$$

Note that Eq. (A3) is applicable to the condition $m > 0$. For the condition $m = 0$, we have $A_{emn} = iE_{mn}a_{m,n}$, $B_{emn} = iE_{mn}b_{m,n}$, and $A_{omn} = B_{omn} = 0$.

The advantage to distinguishing even and odd modes here is that they have one-to-one correspondence with the renormalized dipoles oscillating along the axis directions in Cartesian coordinates. More specifically, under the coordinates defined in the inset of Fig. 4(a), the A_{e11}, A_{o11}, and A_{e01} modes correspond to the renormalized electric dipole oscillating in the x, y, and z directions, respectively, while the B_{e11}, B_{o11}, and B_{e01} modes correspond to the renormalized magnetic dipole oscillating in the x, y, and z directions, respectively.

With the help of these scattering coefficients, the scattering cross section can be evaluated by [23]

$$C_{\rm sca} = \frac{2\pi}{k^2}\sum_{n,m}(2n+1)\left(|A_{emn}|^2 + |A_{omn}|^2 + |B_{emn}|^2 + |B_{omn}|^2\right), \tag{A4}$$

from which we can extract the contributions from the renormalized dipoles as

$$\begin{aligned} C_{\rm sca}^{\overline{p_x}} &= \frac{6\pi}{k^2}|A_{e11}|^2, \quad C_{\rm sca}^{\overline{p_y}} = \frac{6\pi}{k^2}|A_{o11}|^2, \quad C_{\rm sca}^{\overline{p_z}} = \frac{6\pi}{k^2}|A_{e01}|^2, \\ C_{\rm sca}^{\overline{m_x}} &= \frac{6\pi}{k^2}|B_{e11}|^2, \quad C_{\rm sca}^{\overline{m_y}} = \frac{6\pi}{k^2}|B_{o11}|^2, \quad C_{\rm sca}^{\overline{m_z}} = \frac{6\pi}{k^2}|B_{e01}|^2. \end{aligned} \tag{A5}$$

Equation (A5) has been used for the calculation of the results in Figs. 4(a), 5(c), and 7.

APPENDIX B: CALCULATION OF OPTICAL FORCES BASED ON FIELD REPRESENTATION

In this part, we give a detailed description for calculating the optical force using the multipole expansion based on vector spherical functions. The procedure starts from the expansion of the scattered fields by means of vector spherical functions. These are denoted as $\mathbf{N}_{mn}^{(J)}(k,\mathbf{r})$ and $\mathbf{M}_{mn}^{(J)}(k,\mathbf{r})$. Here, n is a positive integer and m is an integer ranging from $-n$ to n. These vector spherical functions are defined as

$$\begin{aligned} \mathbf{N}_{mn}^{(J)}(k,\mathbf{r}) = [\tau_{mn}(\cos\theta)\mathbf{e}_\theta + i\pi_{mn}(\cos\theta)\mathbf{e}_\phi]\frac{[\tilde{z}_n^{(J)}(kr)]'}{kr}\exp(im\phi) \\ + \mathbf{e}_r n(n+1)P_n^m(\cos\theta)\frac{\tilde{z}_n^{(J)}(kr)}{(kr)^2}\exp(im\phi), \end{aligned} \tag{B1}$$

$$\mathbf{M}_{mn}^{(J)}(k,\mathbf{r}) = [i\pi_{mn}(\cos\theta)\mathbf{e}_\theta - \tau_{mn}(\cos\theta)\mathbf{e}_\phi]\frac{\tilde{z}_n^{(J)}(kr)}{kr}\exp(im\phi),$$

where the two auxiliary functions are

$$\pi_{mn}(\cos\theta) = \frac{m}{\sin\theta}P_n^m(\cos\theta), \quad \tau_{mn}(\cos\theta) = \frac{d}{d\theta}P_n^m(\cos\theta), \tag{B2}$$

and the spherical-polar-coordinate-related terms r, θ and ϕ are defined in the inset of Fig. 4(a), k is the wave number in vacuum, $P_n^m(x)$ is the associated Legendre function of the first kind, and $\tilde{z}_n^{(J)}(x) = xz_n^{(J)}(x)$ are Ricatti-Bessel functions, with $z_n^{(J)}(x) = j_n(x), y_n(x), h_n^{(1)}(x)$, and $h_n^{(2)}(x)$ for $J = 1,2,3,4$, respectively. The electric and magnetic scattered fields can then be written as an infinite series of vector spherical functions,

$$\begin{aligned} \mathbf{E}_s &= \sum_{n,m} iE_{mn}\left[a_{mn}\mathbf{N}_{mn}^{(3)}(k,\mathbf{r}) + b_{mn}\mathbf{M}_{mn}^{(3)}(k,\mathbf{r})\right], \\ \mathbf{H}_s &= \frac{k}{\omega\mu_0}\sum_{n,m} E_{mn}\left[b_{mn}\mathbf{N}_{mn}^{(3)}(k,\mathbf{r}) + a_{mn}\mathbf{M}_{mn}^{(3)}(k,\mathbf{r})\right], \end{aligned} \tag{B3}$$

where a_{mn} and b_{mn} are the scattering coefficients for the renormalized electric multipoles and the renormalized magnetic multipoles, respectively. These scattering coefficients can be determined by, taking a_{mn} for instance,

$$a_{mn} = \frac{\int_0^{2\pi}\int_0^{\pi}\mathbf{E}_s\cdot\mathbf{N}_{mn}^{(3)\,*}\sin\theta\, d\theta d\varphi}{iE_{mn}\int_0^{2\pi}\int_0^{\pi}\left|\mathbf{N}_{mn}^{(3)}\right|^2\sin\theta\, d\theta d\varphi}, \tag{B4}$$

Meanwhile, the incident fields can be decomposed, using the coefficients p_{mn} and q_{mn}, as

$$\begin{aligned} \mathbf{E}_i &= -\sum_{n,m} iE_{mn}\left[p_{mn}\mathbf{N}_{mn}^{(1)}(k,\mathbf{r}) + q_{mn}\mathbf{M}_{mn}^{(1)}(k,\mathbf{r})\right], \\ \mathbf{H}_i &= -\frac{k}{\omega\mu_0}\sum_{n,m} E_{mn}\left[q_{mn}\mathbf{N}_{mn}^{(1)}(k,\mathbf{r}) + p_{mn}\mathbf{M}_{mn}^{(1)}(k,\mathbf{r})\right]. \end{aligned} \tag{B5}$$

By combining Eq. (B3) with Eq. (B5), we obtain the explicit expressions for the electric and magnetic total fields, which can be decomposed into a sum of three parts including the incident fields (p_{mn},q_{mn}) and the scattered fields from the renormalized electric multipoles (a_{mn}) and the renormalized magnetic multipoles (b_{mn}). The z component of the optical force can then be derived as [32]

$$F_z = -\frac{4\pi\varepsilon_0}{k^2}|E_0|^2\sum_{n,m}\mathrm{Re}\left(g_{mn}f_{mn}^1 + l_{mn}f_{mn}^2\right), \tag{B6}$$

where we have defined

$$\begin{aligned} g_{mn} &= \left[\frac{n(n+2)(n-m+1)(n+m+1)}{(n+1)^2(2n+1)(2n+3)}\right]^{1/2}, \\ l_{mn} &= \frac{m}{n(n+1)}, \\ f_{mn}^1 &= a_{m,n}a_{m,n+1}^* + b_{m,n}b_{m,n+1}^* - \frac{1}{2}(a_{m,n}p_{m,n+1}^* \\ &\quad + p_{m,n}a_{m,n+1}^* + b_{m,n}q_{m,n+1}^* + q_{m,n}b_{m,n+1}^*), \\ f_{mn}^2 &= a_{m,n}b_{m,n}^* - \frac{1}{2}(p_{m,n}b_{m,n}^* + q_{m,n}a_{m,n}^*). \end{aligned} \tag{B7}$$

From the force expression in Eq. (B6), we can extract the forces acting on the renormalized dipoles and the recoil forces due to dipole interference as

$$F_z^{\bar{\mathbf{p}}} = \frac{2\pi\varepsilon_0}{k^2}|E_0|^2 \sum_{n=1,m} \mathrm{Re}[g_{mn} a_{m,n} p^*_{m,n+1} + l_{mn} q_{m,n} a^*_{m,n}],$$

$$F_z^{\overline{\mathbf{m}}} = \frac{2\pi\varepsilon_0}{k^2}|E_0|^2 \sum_{n=1,m} \mathrm{Re}[g_{mn} b_{m,n} q^*_{m,n+1} + l_{mn} p_{m,n} b^*_{m,n}],$$

$$F_z^{\overline{\mathrm{int}}} = -\frac{4\pi\varepsilon_0}{k^2}|E_0|^2 \sum_{n=1,m} \mathrm{Re}(l_{mn} a_{m,n} b^*_{m,n}). \quad \text{(B8)}$$

[1] Y. B. Zel'dovich, Sov. Phys. JETP **6**, 1184 (1958).
[2] W. C. Haxton, E. M. Henley, and M. J. Musolf, Phys. Rev. Lett. **63**, 949 (1989).
[3] E. E. Radescu and G. Vaman, Phys. Rev. E **65**, 046609 (2002).
[4] A. Ceulemans, L. F. Chibotaru, and P. W. Fowler, Phys. Rev. Lett. **80**, 1861 (1998).
[5] A. Rosado, Phys. Rev. D **61**, 013001 (1999).
[6] I. I. Naumov, L. Bellaiche, and H. Fu, Nature (London) **432**, 737 (2004).
[7] V. M. Dubovik and V. V. Tugushev, Phys. Rep. **187**, 145 (1990).
[8] R. A. Shelby, D. R. Smith, and S. Schultz, Science **292**, 77 (2001).
[9] D. R. Smith, J. B. Pendry, and M. C. K. Wiltshire, Science **305**, 788 (2004).
[10] S. Zhang, Y. S. Park, J. S. Li, X. C. Lu, W. L. Zhang, and X. Zhang, Phys. Rev. Lett. **102**, 023901 (2009).
[11] K. Marinov, A. D. Boardman, V. A. Fedotov, and N. Zheludev, New J. Phys. **9**, 324 (2007).
[12] T. Kaelberer, V. A. Fedotov, N. Papasimakis, D. P. Tsai, and N. I. Zheludev, Science **330**, 1510 (2010).
[13] Y. Huang, W. T. Chen, P. C. Wu, V. Fedotov, V. Savinov, Y. Z. Ho, Y. Chau, N. I. Zheludev, and D. P. Tsai, Opt. Express **20**, 1760 (2012).
[14] B. Ögüt, N. Talebi, R. Vogelgesang, W. Sigle, and P. A. Van Aken, Nano Lett. **12**, 5239 (2012).
[15] V. Savinov, V. A. Fedotov, and N. I. Zheludev, Phys. Rev. B **89**, 205112 (2014).
[16] Q. Zhang, J. J. Xiao, and S. L. Wang, J. Opt. Soc. Am. B **31**, 1103 (2014).
[17] N. Papasimakis, V. A. Fedotov, K. Marinov, and N. I. Zheludev, Phys. Rev. Lett. **103**, 093901 (2009).
[18] Z. G. Dong, J. Zhu, X. Yin, J. Li, C. Lu, and X. G. Zhang, Phys. Rev. B **87**, 245429 (2013).
[19] A. A. Basharin, M. Kafesaki, E. N. Economou, C. M. Soukoulis, V. A. Fedotov, V. Savinov, and N. I. Zheludev, Phys. Rev. X **5**, 011036 (2015).
[20] M. E. Rose, *Multipole Fields* (John Wiley, New York, 1955); J. D. Stratton, *Electromagnetic Theory* (McGraw-Hill, New York, 1941).
[21] J. D. Jackson, *Classical Electrodynamics* (John Wiley& Sons, New York, 1998).
[22] R. E. Raab and O. L. De Lange, *Multipole Theory in Electromagnetism* (Clarendon, Oxford, 2005).
[23] C. F. Bohren and D. R. Huffman, *Absorption and Scattering of Light by Small Particles* (Wiley, New York, 1983).
[24] A. Ashkin, J. M. Dziedzic, J. E. Bjorkholm, and S. Chu, Opt. Lett. **11**, 288 (1986).
[25] P. C. Chaumet, A. Rahmani, and M. Nieto-Vesperinas, Phys. Rev. Lett. **88**, 123601 (2002).
[26] J. Ng, Z. Lin, and C. T. Chan, Phys. Rev. Lett. **104**, 103601 (2010).
[27] M. Nieto-Vesperinas, J. J. Sáenz, R. Gómez-Medina, and L. Chantada, Opt. Express **18**, 11428 (2010).
[28] S. B. Wang, J. Ng, H. Liu, H. H. Zheng, Z. H. Hang, and C. T. Chan, Phys. Rev. B **84**, 075114 (2011).
[29] A. Novitsky, C. W. Qiu, and H. Wang, Phys. Rev. Lett. **107**, 203601 (2011).
[30] J. Chen, J. Ng, Z. Lin, and C. T. Chan, Nat. Photonics **5**, 531 (2011).
[31] S. B. Wang and C. T. Chan, Nat. Commun. **5**, 3307 (2014).
[32] H. Chen, S. Liu, J. Zi, and Z. Lin, ACS Nano. **9**, 1926 (2015).
[33] M. I. Mishchenko, N. T. Zakharov, N. G. Khlebtsov, T. Wriedt, and G. Videen, J. Quant. Spectrosc. Radiat. Transfer. **146**, 349 (2014), and references therein.
[34] J. Ng, Z. F. Lin, C. T. Chan, and P. Sheng, Phys. Rev. B **72**, 085130 (2005).
[35] M. A. Ordal, R. J. Bell, R. W. Alexander, L. L. Long, and M. R. Querry, Appl. Opt. **24**, 4493 (1985).
[36] www.comsol.com.
[37] A. E. Miroshnichenko, A. B. Evlyukhin, Y. F. Yu, R. M. Bakker, A. Chipouline, A. I. Kuznetsov, B. Luk'yanchuk, B. N. Chichkov, and Y. S. Kivshar, Nat. Commun. **6**, 8069 (2015).